(i-Pr-DAB{H,CH_3})] isomers will be formed. The final rearrangement, in which the η^2-coordination of the C(CH_3)=N moiety is replaced by that of the C(H)=N part, is then likely to be very rapid. The fact that only the one isomer with the C(H)=N part being η^2 bonded is obtained is in line with our earlier findings that an η^2-C(H)=N arrangement is thermodynamically more stable than an η^2-C(CH_3)=N one.[1c]

Conclusions

For the first time, mixed-metal carbonyl R-DAB hydride compounds have been isolated.

Neutral R-DAB may be partly reduced to anionic 3-amino-1-azaallyl and reformed again by oxidation; this is accompanied by a hydride migration from the metal carbonyl core to the R-DAB ligand and vice versa.

R-Pyca is able to use its C=N imine bond for η^2-coordination. Thus, just as R-DAB, R-Pyca can act as a six-electron donor in a σ-N,σ-N', η^2-C=N' bonding mode.

Acknowledgment. We thank A. J. M. Duisenberg for collecting the X-ray data, R. Bregman for recording the mass spectra, and J. M. Ernsting for recording the 250-MHz ^{1}H NMR spectra. We thank the Netherland Foundation for Chemical Research (SON) and the Netherland Organization for Pure Research (ZWO) for their financial support.

Registry No. [(μ-H)FeMn(CO)$_6$(p-tol-DAB{H,H})], 94024-85-8; [(μ-H)FeRe(CO)$_6$(i-Pr-DAB{H,H})], 94024-86-9; [(μ-H)FeRe(CO)$_6$(c-Hex-DAB{H,H})], 94024-87-0; [(μ-H)FeRe(CO)$_6$(i-Pr-DAB{Me,Me})], 94024-88-1; [(μ-H)FeMn(CO)$_6$(t-Bu-Pyca)], 94024-89-2; [(μ-H)FeMn(CO)$_6$(i-Pr-Pyca)], 94024-90-5; [(μ-H)FeRe(CO)$_6$(i-Pr-Pyca)], 94024-91-6; [Mn(CO)$_3$(p-tol-DAB{H,H})Br], 70708-87-1; [Re(CO)$_3$(i-Pr-DAB{H,H})Br], 75548-79-7; [Re(CO)$_3$(c-Hex-DAB{H,H})Br], 75548-78-6; [Re(CO)$_3$(i-Pr-DAB{Me,Me})Br], 94024-92-7; [Mn(CO)$_3$(t-Bu-Pyca)Br], 94024-93-8; [Mn(CO)$_3$(i-Pr-Pyca)Br], 94024-94-9; [Re(CO)$_3$(i-Pr-Pyca)Br], 78214-58-1; [FeRe(CO)$_6${(i-Pr)NC(H)C(H)N(H)(i-Pr)}], 91443-27-5; Na[HFe(CO)$_4$], 53558-55-7.

Supplementary Material Available: Listings of observed and calculated structure factors, bond angles, and the final anisotropic thermal parameters, elemental analyses, and an ORTEP drawing of [(μ-H)FeMn(CO)$_6$(t-Bu-Pyca)] (27 pages). Ordering information is given on any current masthead page.

Metal Exchange Reactions under the Influence of a Cyclophosphazene Template: Iron, Cobalt, and Rhodium Metallophosphazenes[1]

Harry R. Allcock,*† Paul R. Suszko,† Linda J. Wagner,† Robert R. Whittle,† and Brian Boso‡

Departments of Chemistry and Physics, The Pennsylvania State University, University Park, Pennsylvania 16802

Received September 4, 1984

The use of a cyclophosphazene ring as a template for the construction of transition-metal dimers or clusters is described. The thermal reactions of a spiro diiron octacarbonyl bonded phosphazene (**2**) with $Co_2(CO)_8$, $CoCp(CO)_2$, or $RhCp(CO)_2$ (Cp = η^5-C_5H_5) lead to the formation of spiro-metallo or metallo cluster phosphazenes in which phosphorus–iron bonds have been replaced by phosphorus–cobalt or phosphorus–rhodium bonds. Reaction of **2** with $Co_2(CO)_8$ yields the mixed-metal cluster **4** in which two cobalt atoms are covalently bound to the bridging phosphazenyl phosphorus atom and the iron atom is coordinatively linked to the ring nitrogen atom. Reaction of **2** with $CoCp(CO)_2$ results in the formation of a phosphazene-bound Fe–Co dimer (**5**) and a phosphazene-bound Co–Co dimer (**6**). Similarly, **2** reacts with $RhCp(CO)_2$ to yield a phosphazene-bound Rh–Rh dimer (**7**). The reaction of **5** with $RhCp(CO)_2$ also leads to the formation of **7**, with no evidence for the formation of any Fe–Rh or Co–Rh dimeric species. The new metallophosphazene compounds were characterized by ^{31}P NMR, Mössbauer, infrared, and mass spectral techniques and by X-ray crystal structure analyses. These small molecule metallophosphazenes are model systems for the corresponding linear high polymers.

Although the field of metal cluster chemistry has been the focus of widespread research during the past 15 years,[2-14] several important questions remain to be answered. Two of these are the subject of this paper. First, how can the synthetic chemist construct mixed-metal clusters with reasonable certainty that specific metals will occupy predetermined sites? It is now well-known *how* hetero metals may be introduced into a cluster, but not known with any certainty *where* they will go. Second, how can the chemist use metal cluster chemistry in conjunction with high polymer chemistry to synthesize macromolecules that have exceptional catalytic or unusual electroactive properties? Possible answers to these questions have become available at the interface between transition metal

† Department of Chemistry.
‡ Department of Physics.

(1) For an earlier paper on organometallic phosphazenes, see: Allcock, H. R.; Lavin, K. D.; Riding, G. H.; Suszko, P. R.; Whittle, R. R. *J. Am. Chem. Soc.* **1984**, *106*, 2337.
(2) Vahrenkamp, H. *Angew. Chem., Int. Ed. Engl.* **1978**, *17*, 379.
(3) Vahrenkamp, H. *Adv. Organomet. Chem.* **1983**, *22*, 169.
(4) Chini, P.; Longini, G.; Albano, V. G. *Adv. Organomet. Chem.* **1976**, *14*, 285.
(5) Chini, P.; Heaton, B. T. *Top. Curr. Chem.* **1977**, *71*, 1.
(6) Chini, P. *J. Organomet. Chem.* **1980**, *200*, 37.
(7) Muetterties, E. L. *Science (Washington, D.C.)* **1977**, *196*, 839.
(8) Muetterties, E. L.; Rhodin, T. N.; Bond, E.; Brucker, C. F.; Pretzer, W. R. *Chem. Rev.* **1979**, *79*, 91.
(9) Muetterties, E. L. *Chem. Eng. News* **1982**, Aug 30, 28.
(10) Pittman, C. V., Jr.; Ryan, R. C. *Chem. Tech.* **1978**, 170.
(11) Ichikawa, M. *J. Catal.* **1979**, *56*, 127.

0276-7333/85/2304-0446$01.50/0

Scheme I

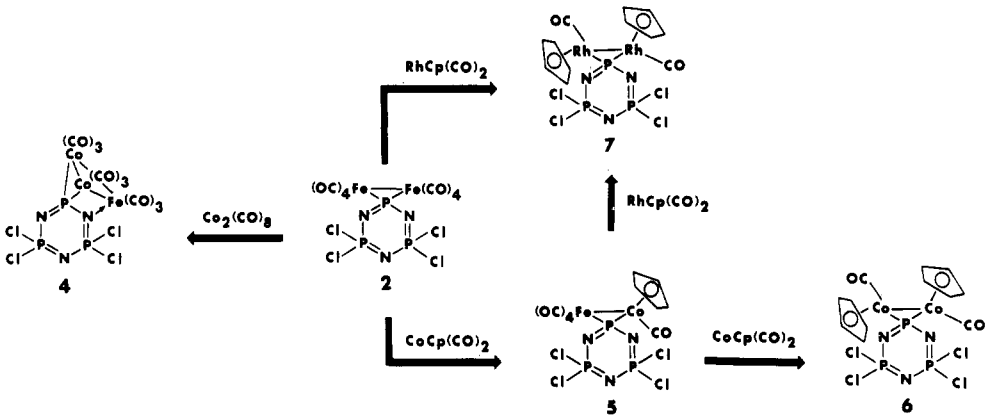

chemistry and the chemistry of main-group ring systems and high polymers.

Cyclo- or polyphosphazenes are unique "carriers" for transition metals. They have the ability to serve as versatile, multifunctional ligands and templates.[15] Small molecule cyclic phosphazenes function as models for probing the behavior of the corresponding linear high polymers. In this paper we describe an approach to answering the two questions through the synthesis and structure determination of a series of new cyclophosphazenes that bear side groups with metal–metal bonds and metal clusters.

Several new approaches have been developed recently in our laboratory that lead to the preparation of cyclophosphazenes with covalent phosphorus–metal bonds.[16-20] One makes use of the reactions of phosphazene anions with transition-metal carbonyl halide compounds.[20] Another involves the nucleophilic substitution reactions of transition-metal carbonyl mono- or dianionic reagents with cyclic halophosphazenes.[16-19] Recently we reported the reaction of hexachlorocyclotriphosphazene $(NPCl_2)_3$ (**1**) with disodium octacarbonyldiferrate(1–), which yields a spiro diiron octacarbonyl bonded phosphazene (**2**) and a triiron decacarbonyl bonded phosphazene (**3**) (eq 1).[18] The

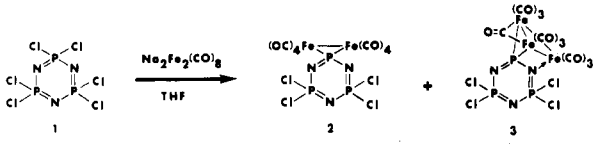

(1)

metallo cluster phosphazene **3** contains both phosphorus–metal and nitrogen–metal bonds, demonstrating both the covalent and coordinative capacities of the phosphazene ring. Compound **3** was also prepared by the thermal reaction of **2** with $Fe(CO)_5$ and $Fe_2(CO)_9$. In addition, we described the preparation of a mixed Fe–Ru metal cluster (**3a**) from the thermal reaction of **2** with $Ru_3(CO)_{12}$ (eq 2).[18b] These reactions provided clues to ways in which metal clusters might be assembled with the use of a phosphazene as a template.

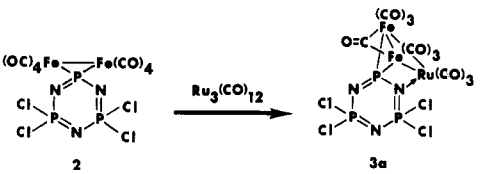

(2)

In this paper we demonstrate the use of compound **2** as an intermediate and template for the formation of new spiro-metallo and metallo cluster phosphazenes that contain both single metal and mixed-metal units. A key feature of these reactions is the ability of one metal to displace another from the P–metal binding site. These reactions allow hetero metals to be introduced into the metallophosphazene in such a way that the disposition of two metals in the cluster depends on their propensity to form covalent bonds to phosphorus or a coordinate bond to skeletal nitrogen. It will be shown that the thermal reactions of **2** with $Co_2(CO)_8$, $CoCp(CO)_2$, or $RhCp(CO)_2$ (Cp = η^5-C_5H_5) lead to the preparation of new metallocyclophosphazenes that possess covalent phosphorus–cobalt and phosphorus–rhodium bonds. Later sections of the paper contain ^{31}P NMR, infrared, Mössbauer, and X-ray diffraction data as evidence in support of the proposed structures of the new compounds.

Results and Discussion

Compound **2** reacts with $Co_2(CO)_8$, $CoCp(CO)_2$, or $RhCp(CO)_2$, to yield spiro-metallo or metallo cluster phosphazenes in which the phosphorus–iron bonds have been replaced by phosphorus–cobalt (**4–6**) or phosphorus–rhodium bonds (**7**) (Scheme I). Compound **5** reacts with $RhCp(CO)_2$ to replace both the phosphorus–iron and phosphorus–cobalt bonds by phosphorus–rhodium bonds to yield the same product as was obtained from the reaction between **2** and $RhCp(CO)_2$. Specific details are as follows.

Reaction of $N_3P_3Cl_4Fe_2(CO)_8$ (2) with $Co_2(CO)_8$. The thermal reaction of **2** with dicobalt octacarbonyl in hexane yields the mixed-metal phosphazene cluster $N_3P_3Cl_4Co_2Fe(CO)_9$ (**4**) (Scheme I). The spectral and analytical data for the product are consistent with the formulation $N_3P_3Cl_4Co_2Fe(CO)_9$ with the two *cobalt* atoms covalently bonded to the bridging phosphazenyl phosphorus atom. Thus, the introduction of the cobalt–carbonyl unit is accompanied by a rearrangement of the metal atoms to yield a product in which an iron–carbonyl fragment has mi-

(12) Geoffroy, G. L. *Acc. Chem. Res.* **1980**, *13*, 469.
(13) Gladfelter, W. L.; Geoffroy, G. L. *Adv. Organomet. Chem.* **1980**, *18*, 207.
(14) Roberts, D. A.; Geoffroy, G. L. In "Comprehensive Organometallic Chemistry"; Wilkinson, G., Stone, F. G. A., Abel, E. W., Eds.; Pergamon Press: Oxford, 1982; Chapter 40.
(15) Allcock, H. R. In "Rings, Clusters, and Polymers of the Main Group Elements"; Cowley, A. H., Ed.; American Chemical Society: Washington, D.C.; 1983; *ACS Symp. Ser.* Chapter 3.
(16) (a) Greigger, P. P.; Allcock, H. R. *J. Am. Chem. Soc.* **1979**, *101*, 2492. (b) Allcock, H. R.; Greigger, P. P.; Wagner, L. J.; Bernheim, M. Y. *Inorg. Chem.* **1981**, *20*, 716.
(17) Allcock, H. R.; Wagner, L. J.; Levin, M. L. *J. Am. Chem. Soc.* **1983**, *105*, 1321.
(18) (a) Suszko, P. R.; Whittle, R. R.; Allcock, H. R. *J. Chem. Soc., Chem. Commun.* **1982**, 649. (b) Allcock, H. R.; Suszko, P. R.; Wagner, L. J.; Whittle, R. R.; Boso, B. *J. Am. Chem. Soc.* **1984**, *106*, 4966.
(19) Allcock, H. R.; Riding, G. H.; Whittle, R. R. *J. Am. Chem. Soc.* **1984**, *106*, 5561.
(20) Nissan, R. A.; Connolly, M. S.; Mirabelli, M. G.; Whittle, R. R.; Allcock, H. R. *J. Chem. Soc., Chem. Commun.* **1983**, 822.

grated to the ring nitrogen atom (along with expulsion of an $Fe(CO)_4$ unit). The active cobalt species in this reaction may be $Co_2(CO)_7$ or $Co_2(CO)_6$, because these intermediates are believed to be involved in the thermal conversion of $Co_2(CO)_8$ to $Co_4(CO)_{12}$.[21] The exact mechanistic pathway for this transformation is a matter for speculation. However, the experimental data are *not* compatible with a random scrambling of both metal atoms between all the possible trimetallo products. Species **4** accounts for approximately 60% of the products generated.

It is interesting that in this reaction the two P–Fe Bonds are replaced by two P–Co bonds without extensive decomposition of the phosphazene ring. Evidently the transition metals serve to stabilize the transition state involved in this conversion. We have previously noted the stabilization of phosphazenyl anions by copper complexation in the reactions of alkyl cuprate systems with $(NPCl_2)_3$.[22] The positioning of the Co_2Fe triad in **4** with respect to the phosphazene ring may reflect a greater tendency for nitrogen to coordinate to iron rather than to cobalt in metal carbonyl compounds. Also, this configuration provides a symmetrical structure with all three metal atoms achieving a closed-shell electronic ground state.

Compound **4** can be isolated as brown plates after recrystallization from toluene or hexane. The compound forms red-brown solutions in common organic solvents and can be chromatographed readily on silica gel with hexane eluent. Compound **4** is quite air-stable in the crystalline state but decomposes slowly in solution on exposure to air. It sublimes at 50–60 °C (0.1 torr).

Reaction of $N_3P_3Cl_4Fe_2(CO)_8$ (2) with $CoCp(CO)_2$. Compound **2** reacts with $CoCp(CO)_2$ in refluxing hexane to yield the mixed-metal dimer $N_3P_3Cl_4FeCoCp(CO)_5$ (**5**) in up to 45% yield, together with a smaller amount of the phosphazene-bound cobalt dimer $N_3P_3Cl_4Co_2Cp_2(CO)_2$ (**6**) (Scheme I). It is known that one or two carbonyl ligands are lost when $CoCp(CO)_2$ reacts with olefins.[23] However, only those products corresponding to the loss of one carbonyl ligand were detected in the reaction of **2** with $CoCp(CO)_2$. No trimetallo clusters were obtained. As in the reaction of **2** with $Co_2(CO)_8$, the preferred pathway involved replacement of iron–phosphorus σ bonds by phosphorus–cobalt σ bonds. The reaction of **5** with an excess of $Fe_2(CO)_9$ under similar conditions results in the partial reversion of **5** to **2**.[24]

The conversion of **2** to **6** appears to be a sequential process proceeding via compound **5**, because treatment of pure **5** with $CoCp(CO)_2$ also results in the formation of **6**. The coordinatively unsaturated CoCp(CO) unit is the reactive cobalt species in these reactions.

Compound **5** is a red-brown crystalline solid that is soluble in THF, toluene, methylene chloride, and chloroform and somewhat soluble in hexane. The material sublimes with partial decomposition (60–70 °C (0.1 torr)). The dicobalt compound (**6**) has similar properties but is only slightly soluble in hydrocarbon solvents. Brown crystals of **6** can be obtained from concentrated toluene solutions on cooling. Both **5** and **6** are air-stable in the crystalline state, but solutions of **5** and **6** decompose slowly in the air.

The stability of these compounds can be understood in terms of their similarity to the diiron derivative **2**. That is, the CoCp(CO) fragment is isoelectric with an $Fe(CO)_4$ unit. Replacement of $Fe(CO)_4$ by a CoCp(CO) unit causes no net change in the electronic disposition about the spiro unit. (The neutral materials $Fe(CO)_5$ and $CoCp(CO)_2$ show similar reactivity patterns, since the iron is considered to be in the (0) oxidation state, whereas the cobalt is in the (+1) oxidation state).

Table I. ^{31}P NMR[a] and Infrared Spectroscopic Data

compound	IR (CO region, hexane), cm^{-1}	^{31}P NMR ($CDCl_3$), δ (J, Hz)
$N_3P_3Cl_4Co_2Fe(CO)_9$, **4**	2102 (s), 2018 (m)	AMX pattern
	2056 (s), 1985 (m)	δ_A 14.0 (J_{AM} = 26)
	2043 (s)	δ_M 25.8 (J_{AX} = 62)
	2031 (m)	δ_X 206.4 (J_{MX} = 26)
$N_3P_3Cl_4FeCoCp(CO)_5$, **5**	2094 (s), 2015 (s)	A_2X pattern
	2038 (s), 2006 (s)	δ_A 11.6 (J_{AX} = 52)
	2028 (s)	δ_X 222.8
$N_3P_3Cl_4Co_2Cp_2(CO)_2$, **6**[b]	1990 (s)	A_2X pattern
		δ_A 10.6 (J_{AX} = 53)
		δ_X 225.2
$N_3P_3Cl_4Rh_2Cp_2(CO)_2$, **7**	2000 (s)	A_2X pattern
		δ_A 10.4 (J_{AX} = 51)
		δ_X 197.1 (J_{XRh_2} = 153)

[a] All spectra are referenced to external H_3PO_4. [b] The IR spectrum for **6** was obtained in CH_2Cl_2.

Reaction of $N_3P_3Cl_4Fe_2(CO)_8$ (2) and $N_3P_3Cl_4FeCoCp(CO)_5$ (5) with $RhCp(CO)_2$. The reactions of **2** and **5** with $RhCp(CO)_2$ in refluxing hexane resulted in the formation of the phosphazene-bound rhodium dimer (**7**) (Scheme I). The spectral and analytical data are consistent with the formulation $N_3P_3Cl_4Rh_2Cp_2(CO)_2$ with the two rhodium atoms covalently bound to the bridging phosphazenyl phosphorus atom. No evidence was obtained that suggested the formation of Fe–Rh or Co–Rh phosphazene mixed-metal dimers and no trimetallo clusters were formed in either case. As in the reactions described above, the preferred pathway appears to involve replacement of phosphorus–iron and phosphorus–cobalt σ bonds by phosphorus–rhodium bonds.

Compound **7** is a red-orange crystalline solid. Its solubility properties are similar to those of compounds **5** and **6**. Red-orange crystals of **7** can be obtained from concentrated cyclohexane/toluene (50:50) solutions on slow cooling. Like compounds **4–6**, compound **7** is air-stable in the crystalline state, but solutions of **7** decompose slowly on exposure to air.

Spectroscopic Characterization. The main point of this paper is the demonstration that the *location* of the different metals within each cluster or spiro structure depends on the response of the metal to opportunities for covalent or coordinate bonding. Hence, it was vital to identify the positions of the metals beyond reasonable doubt. **(a) Infrared Spectra.** The solution infrared spectroscopic data for the carbonyl regions of each of the new metallophosphazenes are summarized in Table I. The data are consistent with the general structures indicated. The solid-state (KBr pellet) infrared spectrum for each compound showed characteristic absorbances for P–N bonds between 1100 and 1250 cm^{-1}. Characteristic absorbances for C–H stretches were also detected for those compounds that possess a cyclopentadienyl ligand.

(21) Ungváry, F.; Marko, L. *Inorg. Chim. Acta* **1970**, *4*, 324.
(22) Allcock, H. R.; Harris, P. J. *J. Am. Chem. Soc.* **1979**, *101*, 6221.
(23) King, R. B.; Treichel, P. M.; Stone, F. G. A. *J. Am. Chem. Soc.* **1961**, *83*, 3593.
(24) Allcock, H. R.; Wagner, L. J.; Schrubbe, G. A., unpublished results to be discussed in a forthcoming publication.

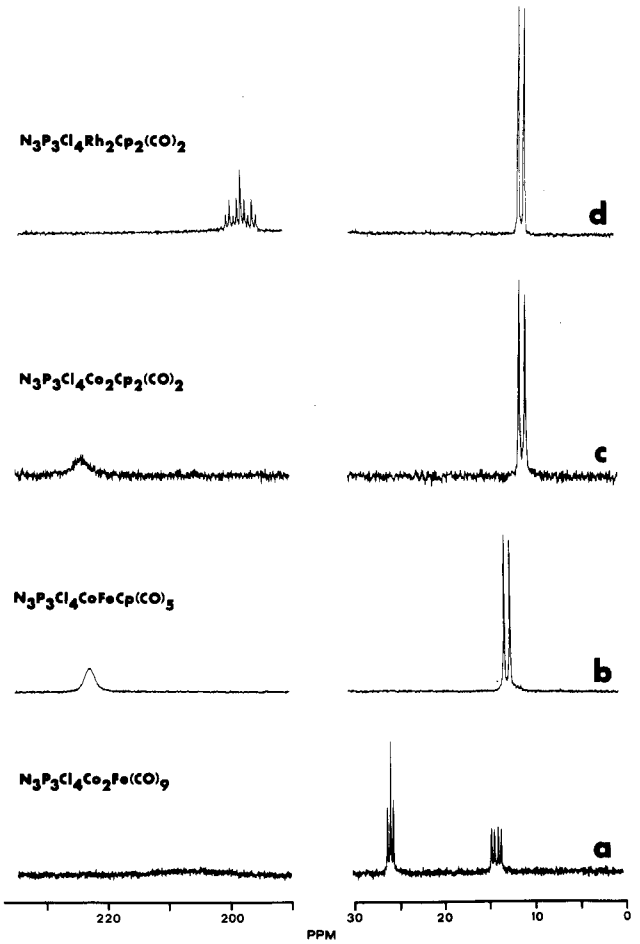

Figure 1. ^{31}P NMR spectra for **4** (spectrum a), **5** (spectrum b), **6** (spectrum c), and **7** (spectrum d).

(b) ^{31}P NMR Spectra. The ^{31}P NMR data for each compound are listed in Table I. The spectra for **4–7** are depicted in Figure 1. All the metallophosphazenes show a large downfield chemical shift for the phosphorus atom attached to the transition metals. This pronounced deshielding effect is partly a consequence of the narrow metal–phosphorus–metal bond angle, which is in the range of 70–80° (see X-ray data). This effect has also been found for other metal–metal bonded fluoro- and chlorophosphazenes.[15–18]

The range of chemical shifts found for the PCl_2 resonances is between +11 and +30 ppm. As in the previously reported iron and ruthenium phosphazene clusters,[18] the lower field resonances within the PCl_2 region for **4** were assigned to the phosphorus atom adjacent to the metal-bound nitrogen (Figure 1). Coordinative electron donation by this nitrogen atom would cause a deshielding of the neighboring phosphorus atom.

For each compound, the different phosphorus environments are well resolved, with no observable second-order effects. The broadened resonances for the metal-bound phosphorus atoms in **4–6** are a result of coupling to the quadrupole cobalt nucleus (Figure 1). In **4**, the PCo_2 resonance is exceptionally broad, indicating a substantial difference in P–Co coupling. The quadrupole relaxation time for the cobalt nuclei in **4** may be shortened by a disruption of the octahedral symmetry about the cobalt atoms. For compound **7**, the rhodium-bound phosphorus atom shows strong coupling to the two rhodium nuclei (J_{PRh_2} = 153 Hz) and measurable coupling to the PCl_2 units.

(c) Mössbauer Spectra. Mössbauer spectroscopy proved to be vital for establishing the location of the iron atom present in **4**. The Mössbauer data for the new iron–cobalt chlorophosphazenes **4** and **5** are listed in Table II, together with the data obtained previously for compounds **2** and **3**.[18] The stack-plotted spectra corresponding to compounds **2–5** are shown in Figure 2.

Table II. Mössbauer Spectroscopic Data for Iron and Iron–Cobalt Metallophosphazenes

	IS,[a] mm/s	QS,[b] mm/s	peak width (Γ) at half height, mm/s	% of total area
$N_3P_3Cl_4FeCoCp(CO)_5$, **5**	0.083	1.267	0.236	100
$N_3P_3Cl_4Fe_2(CO)_8$, **2**	0.103	1.301	0.238	100
$N_3P_3Cl_4Fe_3(CO)_{10}$, **3**	0.263	0.508	0.240	31.2
	0.188	0.859	0.310	68.8
$N_3P_3Cl_4Co_2Fe(CO)_9$, **4**	0.263	0.508	0.241	100

[a] IS = isomer shift. [b] QS = quadrupole splitting.

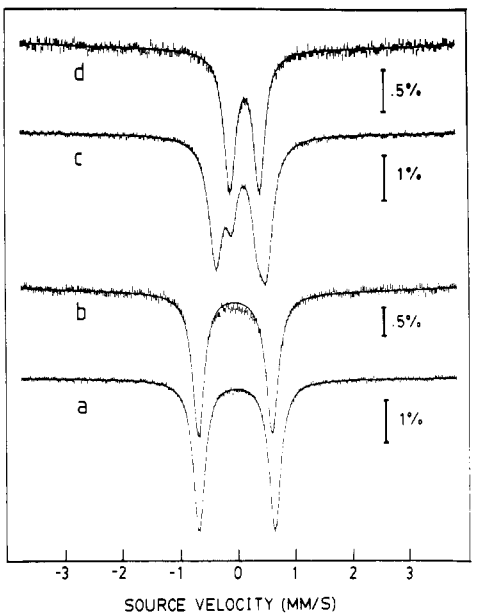

Figure 2. Mössbauer spectra for **5** (spectrum a), **2** (spectrum b), **3** (spectrum c), and **4** (spectrum d).

An inspection of the isomer shift and quadrupole splitting parameters for **2** (Figure 2b) and **5** (Figure 2a) reveals a good agreement. This is strong evidence that the electronic environments about the iron atom are similar in both compounds, as predicted from X-ray diffraction results and other spectroscopic data. The small changes in the isomer shifts and quadrupole splitting that accompany the replacement of one $Fe(CO)_4$ group by a CoCp(CO) group are just barely significant and certainly do not argue for either a charge or spin state change in the remaining iron.

On the basis of elemental analysis of **4** (see Experimental Section), only one iron atom is present per molecule. Thus, only one type of iron species should be detectable. This is consistent with the one doublet shown in Figure 2d. The most important feature of this spectrum is that it is coincident with the smaller doublet in Figure 2c, which corresponds to the nitrogen-bound iron species in **3**. This allows the correct positional assignment to be made for the metal atoms in compound **4**, with the $Fe(CO)_3$ moiety bound to a phosphazene ring nitrogen atom, as in **3**. This distinction could not be made from the X-ray diffraction analysis.

The line widths measured for all the species are essentially equal to the minimum instrumental line width of ~0.230 mm/s; thus, all the samples are homogeneous. The

Table III. Summary of Crystal Data and Intensity Collection Parameters

	4	5	6	7
fw, amu	702.56	596.68	580.83	668.78
space group	$P\bar{1}$	$P\bar{1}$	$P\bar{1}$	$P\bar{1}$
a, Å	7.738 (4)	7.908 (2)	7.957 (1)	7.969 (2)
b, Å	8.711 (4)	9.833 (2)	9.617 (1)	10.143 (2)
c, Å	17.884 (4)	13.486 (3)	14.072 (2)	27.449 (3)
α, deg	75.34 (3)	89.83 (2)	89.46 (1)	87.88 (1)
β, deg	83.21 (3)	88.86 (2)	78.30 (1)	85.63 (1)
γ, deg	71.53 (4)	74.63 (2)	73.04 (1)	70.97 (2)
vol, Å^3	1105.2 (8)	1011.0 (5)	1007.2 (3)	2091.3 (8)
Z	2	2	2	4[b]
d(calcd), g/cm^3	2.111	1.960	1.915	2.124
cryst dimen, mm	0.16 × 0.38 × 0.39	0.14 × 0.28 × 0.28	0.13 × 0.26 × 0.29	0.12 × 0.34 × 0.47
A	1.30	1.20	0.70	1.10
background	0.5	0.5	0.5	0.5
2θ limits, deg	3.0-46.0	3.0-46.4	3.0-44.8	3.2-44.2
data measd	3083	2874	2601	5190
unique nonzero data	2718	2587	2396	4795
observed data ($I > 2\sigma(I)$)	2590	2459	2306	4690
μ, cm^{-1}	29.5	23.74	24.85	23.11
R_1/R_2	0.070/0.072	0.051/0.058	0.033/0.037	0.048/0.055
goodness of fit	1.524	1.621	1.180	3.444
data/parameter	9.25	10.08	9.81	9.96
drift correction	0.994-2.431	0.956-1.320	0.940-1.032	0.988-1.045
recrystn solvent	toluene	toluene	toluene	cyclohexane/toluene
largest residual peak,[a] e Å^{-3}	0.15	0.07	0.05	0.19

[a] Peak residuals are given relative to the intensity of a carbon atom (C, 6 e Å^{-3}). [b] The two molecules in the asymmetric unit differ only by a small change in conformation, presumably induced by crystal packing forces.

Table IV. Bond Lengths (Å) for 4

Co(1)-Co(2)	2.561 (2)	P(3)-Cl(3)	1.976 (5)
Co(1)-Fe	2.653 (2)	P(3)-Cl(4)	1.996 (5)
Co(2)-Fe	2.642 (2)	P(1)-N(1)	1.671 (6)
Co(1)-P(1)	2.134 (3)	P(1)-N(3)	1.625 (8)
Co(2)-P(1)	2.124 (2)	P(2)-N(1)	1.554 (7)
Fe-N(1)	2.055 (8)	P(3)-N(3)	1.527 (7)
Co(1)-C(1)	1.81 (1)	P(2)-N(2)	1.568 (9)
Co(1)-C(2)	1.84 (1)	P(3)-N(2)	1.595 (6)
Co(1)-C(3)	1.79 (1)	C(1)-O(1)	1.12 (1)
Co(2)-C(4)	1.81 (1)	C(2)-O(2)	1.13 (2)
Co(2)-C(5)	1.82 (1)	C(3)-O(3)	1.12 (1)
Co(2)-C(6)	1.77 (1)	C(4)-O(4)	1.11 (1)
Fe-C(7)	1.75 (1)	C(5)-O(5)	1.11 (1)
Fe-C(8)	1.82 (1)	C(6)-O(6)	1.14 (1)
Fe-C(9)	1.83 (1)	C(7)-O(7)	1.15 (2)
P(2)-Cl(1)	1.969 (3)	C(8)-O(8)	1.13 (1)
P(2)-Cl(2)	1.985 (4)	C(9)-O(9)	1.12 (1)

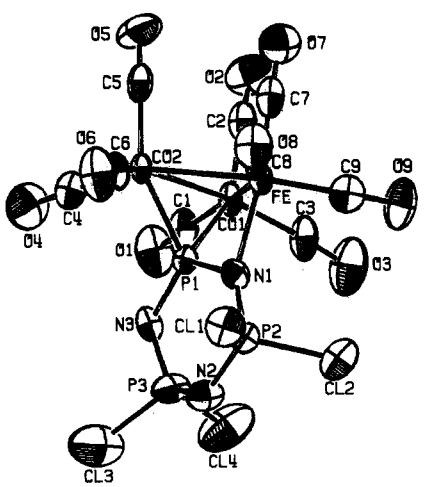

Figure 3. ORTEP diagram for compound 4.

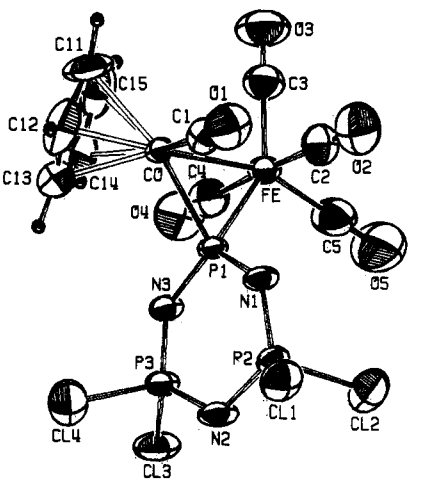

Figure 4. ORTEP diagram for compound 5.

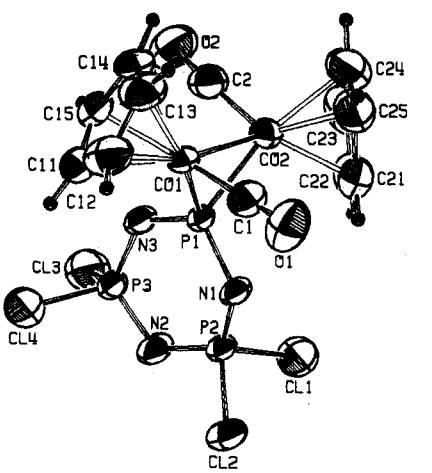

Figure 5. ORTEP diagram for compound 6.

isomer shifts did not allow the unambiguous assignment of valence and spin values to the iron species. However, high-spin ferrous species can be ruled out.

X-ray Structure Analyses: General Data. A single-crystal X-ray structure determination was carried out for each of the new metallophosphazenes 4–7. The main crystallographic details are summarized in Table III. Bond lengths, bond angles, and atomic positional parameters are listed in Tables IV–XV.[25] The tables of thermal

Table V. Bond Angles (deg) for 4

Co(2)-Co(1)-Fe	60.85 (5)	Co(1)-Co(2)-C(5)	97.0 (3)	C(1)-Co(1)-C(2)	96.3 (4)
Co(1)-Co(2)-Fe	61.30 (5)	Co(1)-Co(2)-C(6)	143.3 (3)	C(1)-Co(1)-C(3)	104.2 (4)
Co(1)-Fe-Co(2)	57.85 (5)	Fe-Co(2)-C(4)	158.1 (3)	C(2)-Co(1)-C(3)	104.7 (4)
Co(2)-Co(1)-P(1)	52.85 (7)	Fe-Co(2)-C(5)	99.3 (3)	C(4)-Co(2)-C(5)	98.4 (4)
Co(1)-Co(2)-P(1)	53.21 (8)	Fe-Co(2)-C(6)	85.5 (3)	C(4)-Co(2)-C(6)	102.6 (5)
Fe-Co(1)-P(1)	63.84 (7)	P(1)-Co(2)-C(4)	94.2 (3)	C(5)-Co(2)-C(6)	103.9 (4)
Fe-Co(2)-P(1)	64.17 (8)	P(1)-Co(2)-C(5)	149.8 (3)	C(7)-Fe-C(8)	93.0 (4)
Co(1)-Fe-N(1)	81.9 (2)	P(1)-Co(2)-C(6)	99.9 (3)	C(7)-Fe-C(9)	93.0 (5)
Co(2)-Fe-N(1)	82.0 (2)	Co(1)-Fe-C(7)	87.7 (3)	C(8)-Fe-C(9)	94.9 (4)
Co(1)-P(1)-Co(2)	73.94 (9)	Co(1)-Fe-C(8)	162.6 (3)	N(1)-P(1)-N(3)	110.1 (4)
Co(1)-P(1)-N(1)	109.5 (3)	Co(1)-Fe-C(9)	102.4 (3)	N(1)-P(2)-N(2)	115.7 (4)
Co(1)-P(1)-N(3)	122.9 (2)	Co(2)-Fe-C(7)	87.6 (3)	N(2)-P(3)-N(3)	120.0 (4)
Co(2)-P(1)-N(1)	109.7 (2)	Co(2)-Fe-C(8)	104.8 (3)	P(1)-N(1)-P(2)	127.4 (5)
Co(2)-P(1)-N(3)	126.0 (3)	Co(2)-Fe-C(9)	160.3 (3)	P(2)-N(2)-P(3)	119.0 (5)
Fe-N(1)-P(1)	86.5 (3)	N(1)-Fe-C(7)	168.2 (3)	P(1)-N(3)-P(3)	121.8 (4)
Fe-N(1)-P(2)	146.0 (4)	N(1)-Fe-C(8)	95.2 (4)	Cl(1)-P(2)-Cl(2)	102.1 (1)
Co(2)-Co(1)-C(1)	99.7 (3)	N(1)-Fe-C(9)	94.8 (4)	Cl(3)-P(3)-Cl(4)	101.3 (2)
Co(2)-Co(1)-C(2)	97.8 (3)	Co(1)-C(1)-O(1)	175.7 (10)	Cl(1)-P(2)-N(1)	110.1 (3)
Co(2)-Co(1)-C(3)	144.9 (3)	Co(1)-C(2)-O(2)	176.8 (8)	Cl(1)-P(2)-N(2)	108.9 (3)
Fe-Co(1)-C(1)	155.0 (4)	Co(1)-C(3)-O(3)	176.2 (12)	Cl(2)-P(2)-N(1)	108.7 (4)
Fe-Co(1)-C(2)	101.6 (3)	Co(2)-C(4)-O(4)	177.8 (9)	Cl(2)-P(2)-N(2)	110.4 (3)
Fe-Co(1)-C(3)	88.1 (3)	Co(2)-C(5)-O(5)	178.9 (10)	Cl(3)-P(3)-N(2)	106.8 (4)
P(1)-Co(1)-C(1)	92.2 (4)	Co(2)-C(6)-O(6)	176.9 (11)	Cl(3)-P(3)-N(3)	109.5 (3)
P(1)-Co(1)-C(2)	150.5 (3)	Fe-C(7)-O(7)	175.4 (8)	Cl(4)-P(3)-N(2)	107.6 (3)
P(1)-Co(1)-C(3)	100.4 (4)	Fe-C(8)-O(8)	176.7 (10)	Cl(4)-P(3)-N(3)	109.8 (3)
Co(1)-Co(2)-C(4)	103.8 (3)	Fe-C(9)-O(9)	176.9 (8)		

Table VI. Fractional Atomic Positional Parameters for 4

	x	*y*	*z*
Co(1)	0.5560 (2)	0.2866 (1)	0.17296 (7)
Co(2)	0.8916 (2)	0.2178 (1)	0.12627 (6)
Fe	0.7663 (2)	−0.0264 (1)	0.20718 (7)
Cl(1)	1.1246 (4)	−0.1832 (3)	0.3910 (1)
Cl(2)	0.7237 (4)	−0.1219 (3)	0.4490 (1)
Cl(3)	0.9634 (5)	0.4540 (3)	0.4022 (2)
Cl(4)	0.5791 (5)	0.4138 (4)	0.4233 (2)
P(1)	0.7864 (3)	0.2381 (2)	0.2397 (1)
P(2)	0.8900 (4)	−0.0057 (3)	0.3829 (1)
P(3)	0.8230 (4)	0.3251 (3)	0.3734 (1)
N(1)	0.827 (1)	0.0487 (7)	0.2983 (4)
N(2)	0.907 (1)	0.1363 (8)	0.4181 (4)
N(3)	0.809 (1)	0.3691 (7)	0.2857 (4)
O(1)	0.476 (1)	0.6447 (8)	0.1576 (4)
O(2)	0.393 (1)	0.3083 (9)	0.0267 (4)
O(3)	0.301 (1)	0.1964 (10)	0.2968 (5)
O(4)	0.962 (1)	0.5389 (8)	0.0898 (4)
O(5)	0.839 (1)	0.1976 (9)	−0.0302 (4)
O(6)	1.255 (1)	−0.0096 (8)	0.1614 (4)
O(7)	0.670 (1)	−0.0725 (8)	0.0640 (4)
O(8)	1.080 (1)	−0.3289 (8)	0.2198 (4)
O(9)	0.520 (1)	−0.2070 (9)	0.3005 (4)
C(1)	0.503 (1)	0.509 (1)	0.1610 (5)
C(2)	0.459 (1)	0.296 (1)	0.0822 (6)
C(3)	0.397 (1)	0.229 (1)	0.2474 (6)
C(4)	0.936 (1)	0.417 (1)	0.1022 (5)
C(5)	0.857 (1)	0.206 (1)	0.0288 (6)
C(6)	1.111 (1)	0.076 (1)	0.1480 (5)
C(7)	0.707 (1)	−0.048 (1)	0.1195 (6)
C(8)	0.962 (1)	−0.211 (1)	0.2162 (5)
C(9)	0.610 (1)	−0.135 (1)	0.2641 (6)

parameters,[26] root-mean-square displacements, and F_o and F_c values are available as supplementary material. Labeled ORTEP drawings for each structure are shown in Figures 3–6.

Structure of 4. The positions of the two cobalt atoms relative to the iron atom in 4 could not be unequivocally determined by X-ray crystallography due to the small differences between these atoms. The location of the different metal atoms was based on the Mössbauer spectroscopic analysis, as described in the previous section.

Compound 4 was found to possess an overall trimetallophosphazene framework analogous to those of the iron and iron–ruthenium clusters 3[18] (Figure 3). However, each metal atom in 4 is ligated by three terminal carbonyl groups, whereas compounds 3 possess an additional

Table VII. Bond Lengths (Å) for 5

Co-Fe	2.647 (2)	P(1)-N(1)	1.622 (7)
Co-P(1)	2.149 (2)	P(1)-N(3)	1.639 (8)
Fe-P(1)	2.220 (2)	P(2)-N(1)	1.562 (6)
Co-C(11)	2.07 (1)	P(3)-N(3)	1.543 (6)
Co-C(12)	2.06 (1)	P(2)-N(2)	1.583 (8)
Co-C(13)	2.07 (1)	P(3)-N(2)	1.591 (7)
Co-C(14)	2.08 (1)	C(1)-O(1)	1.11 (1)
Co-C(15)	2.08 (1)	C(2)-O(2)	1.11 (2)
Co-C(1)	1.77 (1)	C(3)-O(3)	1.13 (1)
Fe-C(2)	1.84 (1)	C(4)-O(4)	1.10 (2)
Fe-C(3)	1.81 (1)	C(5)-O(5)	1.14 (2)
Fe-C(4)	1.84 (1)	C(11)-C(12)	1.43 (2)
Fe-C(5)	1.79 (1)	C(11)-C(15)	1.38 (2)
P(2)-Cl(1)	1.985 (3)	C(12)-C(13)	1.35 (2)
P(2)-Cl(2)	2.007 (4)	C(13)-C(14)	1.39 (2)
P(3)-Cl(3)	1.990 (4)	C(14)-C(15)	1.32 (2)
P(3)-Cl(4)	2.019 (4)		

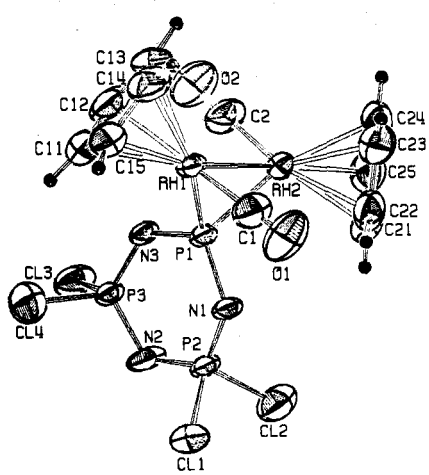

Figure 6. ORTEP diagram for compound 7.

(25) The number in parentheses following each numerical entry in Tables IV–XV represents the estimated standard deviation (according to the uncertainty in the last digit) of the value.

(26) The form of the anisotropic thermal parameter is $\exp[-2\pi^2(U_{11}a^{*2}h^2 + U_{22}b^{*2}k^2 + U_{33}c^{*2}l^2 + 2U_{12}a^*b^*hk + 2U_{13}a^*c^*hl + 2U_{23}b^*c^*kl)]$. The units of the values are in 10^3 Å^2.

Table VIII. Bond Angles (deg) for 5

Fe-Co-P(1)	53.94 (6)	N(1)-P(1)-N(3)	111.7 (3)	Fe-C(2)-O(2)	175.8 (9)
Co-Fe-P(1)	51.51 (6)	N(1)-P(2)-N(2)	120.0 (4)	Fe-C(3)-O(3)	179.0 (16)
Co-P(1)-Fe	74.55 (7)	N(2)-P(3)-N(3)	121.0 (4)	Fe-C(4)-O(4)	176.7 (10)
Co-P(1)-N(1)	117.1 (3)	P(1)-N(1)-P(2)	123.3 (5)	Fe-C(5)-O(5)	177.3 (14)
Co-P(1)-N(3)	115.3 (2)	P(2)-N(2)-P(3)	116.8 (4)	C(2)-Fe-C(3)	91.4 (5)
Fe-P(1)-N(1)	114.7 (3)	P(1)-N(3)-P(3)	123.2 (4)	C(2)-Fe-C(4)	177.0 (5)
Fe-P(1)-N(3)	119.0 (3)	Cl(1)-P(2)-Cl(2)	100.0 (1)	C(2)-Fe-C(5)	89.4 (6)
Fe-Co-C(1)	100.5 (3)	Cl(3)-P(3)-Cl(4)	99.8 (2)	C(3)-Fe-C(4)	91.4 (5)
Co-Fe-C(2)	85.5 (3)	Cl(1)-P(2)-N(1)	108.9 (3)	C(3)-Fe-C(5)	110.2 (5)
Co-Fe-C(3)	94.9 (3)	Cl(1)-P(2)-N(2)	107.0 (3)	C(4)-Fe-C(5)	90.6 (6)
Co-Fe-C(4)	93.2 (3)	Cl(2)-P(2)-N(1)	111.2 (3)	C(12)-C(11)-C(15)	106 (1)
Co-Fe-C(5)	154.5 (3)	Cl(2)-P(2)-N(2)	107.9 (3)	C(11)-C(12)-C(13)	106 (1)
P(1)-Co-C(1)	91.6 (3)	Cl(3)-P(3)-N(2)	108.8 (3)	C(12)-C(13)-C(14)	109 (1)
P(1)-Fe-C(2)	88.8 (3)	Cl(3)-P(3)-N(3)	108.9 (3)	C(13)-C(14)-C(15)	109 (1)
P(1)-Fe-C(3)	146.3 (3)	Cl(4)-P(3)-N(2)	105.6 (3)	C(11)-C(15)-C(14)	109 (1)
P(1)-Fe-C(4)	88.3 (3)	Cl(4)-P(3)-N(3)	110.5 (3)		
P(1)-Fe-C(5)	103.5 (4)	Co-C(1)-O(1)	174.8 (8)		

Table IX. Fractional Atomic Positional Parameters for 5

	x	y	z
Fe	0.6490 (2)	0.2021 (1)	0.1250 (1)
Co	0.7004 (1)	0.1479 (1)	0.3160 (1)
P(1)	0.5576 (3)	0.3452 (2)	0.2534 (2)
P(2)	0.2368 (3)	0.5485 (2)	0.2816 (2)
P(3)	0.5379 (3)	0.6224 (2)	0.3108 (2)
Cl(1)	0.0418 (3)	0.5591 (3)	0.3788 (2)
Cl(2)	0.0992 (4)	0.6132 (3)	0.1588 (2)
Cl(3)	0.6233 (4)	0.7728 (2)	0.2438 (2)
Cl(4)	0.6054 (3)	0.6491 (3)	0.4516 (2)
N(1)	0.3467 (8)	0.3916 (7)	0.2715 (6)
N(2)	0.3292 (9)	0.6664 (7)	0.3155 (6)
N(3)	0.6436 (8)	0.4776 (7)	0.2702 (6)
O(1)	0.3846 (9)	0.0760 (8)	0.3775 (6)
O(2)	0.3357 (12)	0.0949 (9)	0.1463 (6)
O(3)	0.8626 (12)	−0.0768 (9)	0.0582 (7)
O(4)	0.9505 (11)	0.3222 (9)	0.1003 (6)
O(5)	0.4774 (17)	0.3688 (10)	−0.0421 (7)
C(1)	0.5037 (12)	0.1044 (10)	0.3495 (6)
C(2)	0.4541 (15)	0.1360 (11)	0.1420 (7)
C(3)	0.7791 (15)	0.0302 (11)	0.0836 (8)
C(4)	0.8390 (15)	0.2761 (11)	0.1123 (8)
C(5)	0.5479 (18)	0.3038 (12)	0.0217 (8)
C(11)	0.8810 (18)	−0.0157 (11)	0.3842 (14)
C(12)	0.8104 (14)	0.0966 (16)	0.4524 (9)
C(13)	0.8584 (15)	0.2099 (11)	0.4174 (9)
C(14)	0.9523 (14)	0.1736 (15)	0.3288 (9)
C(15)	0.9641 (15)	0.0400 (18)	0.3091 (9)
H(11)	0.8726	−0.1121	0.3894
H(12)	0.7414	0.0924	0.5122
H(13)	0.8316	0.3019	0.4490
H(14)	1.0011	0.2362	0.2881
H(15)	1.0220	−0.0113	0.2510

bridging carbonyl between the phosphorus-bound metal atoms. With the absence of a bridging carbonyl group, the $Co_2Fe(CO)_9$ unit is isoelectronic with a $Fe_3(CO)_{10}$ or a $Fe_2Ru(CO)_{10}$ unit. Thus, as in compounds **3**, phosphazene ring functions as a net four-electron donor in **4**. Dahl et al. have described the structure of a related sulfur-capped cluster, $FeCo_2(CO)_9S$,[27] in which the sulfur atom plays the same role as the phosphazene ring in **4**.

The structural features of compound **4** are very similar to those described for compounds **3**.[18] The phosphazene ring in **4** shows some deviation from planarity ($\chi^2 = 1140$). The distorted phosphazene plane passes close to the Fe(3) atom (0.22 Å) and bisects the Co(1)–Co(2) segment. The P(1)–Co(2)–Co(1) plane is tilted away from the P(1)–N(2) axis (11.2°). The plane defined by the three metal atoms forms a dihedral angle of 77.8° with the P(1)–Co(2)–Co(1) plane.

(27) Stevenson, D. L.; Wei, C. H.; Dahl, L. F. *J. Am. Chem. Soc.* **1971**, *93*, 6027.

Table X. Bond Lengths (Å) for 6

Co(1)-Co(2)	2.552 (1)	P(1)-N(1)	1.643 (4)
Co(1)-P(1)	2.144 (2)	P(1)-N(3)	1.638 (5)
Co(2)-P(1)	2.142 (2)	P(2)-N(1)	1.565 (5)
Co(1)-C(1)	1.732 (8)	P(3)-N(3)	1.563 (5)
Co(1)-C(11)	2.066 (8)	P(2)-N(2)	1.583 (6)
Co(1)-C(12)	2.058 (7)	P(3)-N(2)	1.575 (4)
Co(1)-C(13)	2.087 (7)	C(1)-O(1)	1.14 (1)
Co(1)-C(14)	2.094 (6)	C(2)-O(2)	1.14 (1)
Co(1)-C(15)	2.065 (6)	C(11)-C(12)	1.39 (1)
Co(2)-C(2)	1.732 (8)	C(11)-C(15)	1.41 (1)
Co(2)-C(21)	2.076 (7)	C(12)-C(13)	1.42 (1)
Co(2)-C(22)	2.069 (7)	C(13)-C(14)	1.37 (1)
Co(2)-C(23)	2.099 (9)	C(14)-C(15)	1.41 (1)
Co(2)-C(24)	2.096 (9)	C(21)-C(22)	1.41 (1)
Co(2)-C(25)	2.070 (7)	C(21)-C(25)	1.38 (1)
P(2)-Cl(1)	2.019 (2)	C(22)-C(23)	1.41 (1)
P(2)-Cl(2)	1.994 (2)	C(23)-C(24)	1.38 (1)
P(3)-Cl(3)	1.990 (3)	C(24)-C(25)	1.43 (1)
P(3)-Cl(4)	2.005 (3)		

A Co(1)–Co(2) distance of 2.561 Å was found in **4**, compared to an average Co–Fe length of 2.647 Å. (In the disordered structure of $FeCo_2(CO)_9S$ reported by Dahl, an average metal–metal bond length of 2.554 Å was found.[27]) The P(1)–Co bond lengths average 2.129 Å, and the Fe(3)–N(1) distance of 2.055 Å is consistent with a coordinative bond, N → Fe.

The presence of the trimetallo moiety causes a disruption of the bond length symmetry in the phosphazene skeleton of **4**. The P(1)–N(1) length in **4** is 1.671 Å, and this is the longest P–N bond in the structure. The adjacent P(1)–N(3) bond length is 1.625 Å, whereas the remaining P–N bonds are in the range 1.53–1.60 Å. As was observed for other metallophosphazene compounds,[16-18] the smallest endocyclic angle in the phosphazene ring is centered at P(1), with a value of 110.1°. The Co(1)–P(1)–Co(2) angle is 73.9°. As in compounds **3**, the largest endocyclic phosphazene ring angle in **4** is P(1)–N(1)–P(2) (127.4°). The remaining endocyclic phosphazene ring angles lie in the range 115.7–121.8°. Other bond lengths and bond angles are given in Table IV and Table V, respectively.

Structures of 5–7. The X-ray structure analyses of **5–7** revealed that each compound also contains a geminal pair of metal atoms, with metal–metal bonds forming part of a three-membered spiro ring and with a phosphorus atom at the spiro juncture.

The molecular structure of **5** contains an Fe–P(1)–Co spiro unit, with a cyclopentadienyl ring and one carbonyl ligand bound to the cobalt atom, and four carbonyl ligands linked to the iron atom (Figure 4). The orientation of the four iron-bound carbonyl ligands in **5** is similar to that reported for the diiron species **2**.[18] This results in a distorted octahedral arrangement about the iron atom. As

Table XI. Bond Angles (deg) for 6

Co(1)-Co(2)-P(1)	53.49 (5)	N(2)-P(3)-N(3)	120.4 (3)	Cl(4)-P(3)-N(3)	111.3 (2)
Co(2)-Co(1)-P(1)	53.43 (5)	P(1)-N(1)-P(2)	121.9 (3)	Co(1)-C(1)-O(1)	176.2 (6)
Co(1)-P(1)-Co(2)	73.09 (6)	P(2)-N(2)-P(3)	116.6 (3)	Co(2)-C(2)-O(2)	177.1 (7)
Co(1)-P(1)-N(1)	117.0 (2)	P(1)-N(3)-P(3)	122.9 (3)	C(12)-C(11)-C(15)	108.1 (7)
Co(1)-P(1)-N(3)	117.0 (2)	Cl(1)-P(2)-Cl(2)	100.2 (1)	C(11)-C(12)-C(13)	107.3 (8)
Co(2)-P(1)-N(1)	116.8 (2)	Cl(3)-P(3)-Cl(4)	100.3 (1)	C(12)-C(13)-C(14)	108.8 (8)
Co(2)-P(1)-N(3)	117.0 (2)	Cl(1)-P(2)-N(1)	109.9 (2)	C(13)-C(14)-C(15)	108.2 (6)
Co(1)-Co(2)-C(2)	91.2 (2)	Cl(1)-P(2)-N(2)	108.0 (3)	C(11)-C(15)-C(14)	107.6 (7)
Co(2)-Co(1)-C(1)	90.9 (2)	Cl(2)-P(2)-N(1)	109.3 (2)	C(22)-C(21)-C(25)	108.3 (7)
P(1)-Co(1)-C(1)	95.4 (2)	Cl(2)-P(2)-N(2)	106.7 (2)	C(21)-C(22)-C(23)	107.4 (7)
P(1)-Co(2)-C(2)	95.0 (2)	Cl(3)-P(3)-N(2)	106.6 (3)	C(22)-C(23)-C(24)	108.7 (8)
N(1)-P(1)-N(3)	111.3 (2)	Cl(3)-P(3)-N(3)	109.1 (2)	C(23)-C(24)-C(25)	107.6 (7)
N(1)-P(2)-N(2)	120.8 (2)	Cl(4)-P(3)-N(2)	107.2 (2)	C(21)-C(25)-C(24)	108.0 (8)

Table XII. Fractional Atomic Positional Parameters for 6

	x	*y*	*z*
Co(1)	0.4822 (1)	0.14537 (8)	0.33993 (6)
Co(2)	0.5599 (1)	0.11956 (8)	0.15464 (6)
P(1)	0.5113 (2)	−0.0440 (1)	0.2516 (1)
P(2)	0.6775 (2)	−0.3456 (2)	0.2384 (1)
P(3)	0.3168 (2)	−0.2481 (2)	0.2734 (1)
Cl(1)	0.8126 (3)	−0.4233 (2)	0.1029 (1)
Cl(2)	0.8315 (2)	−0.4795 (2)	0.3168 (1)
Cl(3)	0.1560 (3)	−0.2954 (2)	0.1956 (2)
Cl(4)	0.1780 (3)	−0.2554 (2)	0.4083 (2)
N(1)	0.6836 (6)	−0.1868 (5)	0.2556 (4)
N(2)	0.4921 (6)	−0.3818 (5)	0.2573 (5)
N(3)	0.3293 (6)	−0.0912 (5)	0.2521 (4)
O(1)	0.8531 (7)	0.0775 (6)	0.3520 (4)
O(2)	0.1920 (8)	0.2484 (6)	0.1418 (4)
C(1)	0.7076 (10)	0.1035 (7)	0.3439 (5)
C(2)	0.3365 (10)	0.1964 (7)	0.1493 (5)
C(11)	0.2664 (10)	0.1484 (8)	0.4580 (6)
C(12)	0.3799 (12)	0.2145 (9)	0.4836 (5)
C(13)	0.3832 (11)	0.3373 (8)	0.4278 (6)
C(14)	0.2783 (9)	0.3442 (6)	0.3610 (5)
C(15)	0.2054 (8)	0.2263 (7)	0.3733 (5)
C(21)	0.7721 (10)	−0.0006 (8)	0.0479 (5)
C(22)	0.8379 (9)	0.0512 (8)	0.1217 (5)
C(23)	0.7785 (10)	0.2049 (8)	0.1237 (5)
C(24)	0.6746 (11)	0.2470 (8)	0.0552 (6)
C(25)	0.6693 (12)	0.1178 (10)	0.0079 (5)

Table XIII. Bond Lengths (Å) for 7

	A	B
Rh(1)-Rh(2)	2.767 (1)	2.728 (1)
Rh(1)-P(1)	2.265 (3)	2.195 (3)
Rh(2)-P(1)	2.203 (3)	2.274 (3)
Rh(1)-C(1)	1.88 (1)	1.87 (1)
Rh(1)-C(11)	2.24 (1)	2.22 (1)
Rh(1)-C(12)	2.22 (1)	2.24 (1)
Rh(1)-C(13)	2.28 (1)	2.23 (1)
Rh(1)-C(14)	2.30 (1)	2.23 (2)
Rh(1)-C(15)	2.23 (1)	2.26 (2)
Rh(2)-C(2)	1.84 (1)	1.85 (1)
Rh(2)-C(21)	2.26 (1)	2.23 (1)
Rh(2)-C(22)	2.24 (1)	2.22 (2)
Rh(2)-C(23)	2.26 (2)	2.23 (1)
Rh(2)-C(24)	2.24 (1)	2.29 (2)
Rh(2)-C(25)	2.23 (1)	2.32 (1)
P(2)-Cl(1)	1.973 (5)	1.993 (5)
P(2)-Cl(2)	2.046 (5)	2.002 (5)
P(3)-Cl(3)	1.986 (5)	1.973 (4)
P(3)-Cl(4)	2.022 (5)	2.022 (5)
P(1)-N(1)	1.623 (7)	1.64 (1)
P(1)-N(3)	1.63 (1)	1.646 (8)
P(2)-N(1)	1.54 (1)	1.55 (1)
P(3)-N(3)	1.53 (1)	1.55 (1)
P(2)-N(2)	1.59 (1)	1.587 (8)
P(3)-N(2)	1.600 (8)	1.59 (1)
C(1)-O(1)	1.11 (2)	1.11 (2)
C(2)-O(2)	1.13 (2)	1.12 (2)
C(11)-C(12)	1.38 (2)	1.40 (2)
C(11)-C(15)	1.36 (2)	1.43 (2)
C(12)-C(13)	1.48 (2)	1.40 (2)
C(13)-C(14)	1.36 (2)	1.48 (2)
C(14)-C(15)	1.39 (2)	1.34 (2)
C(21)-C(22)	1.45 (2)	1.32 (2)
C(21)-C(25)	1.33 (2)	1.46 (3)
C(22)-C(23)	1.39 (2)	1.41 (2)
C(23)-C(24)	1.39 (2)	1.40 (3)
C(24)-C(25)	1.43 (3)	1.34 (3)

in **2**, a "bent" metal–metal bond[28,29] can be visualized in **5**, completing the approximately octahedral coordination about each metal atom. The Fe–Co distance of 2.647 Å in **5** is slightly longer than the average Fe–Co distance quoted for related compounds (2.555 Å).[14] Vahrenkamp has reported a trimetallo compound, $(NO)_2Fe[P(CH_3)_2]_2Fe(CO)_2[P(CH_3)_2]Co(CO)_3$, with a similar Fe–Co distance (2.66 Å).[30] The plane of the cyclopentadienyl ring in **5** is tilted off to one side of the Fe–Co axis: the cyclopentadienyl ring forms a dihedral angle of 47.8° with the Fe–P(1)–Co plane and an angle of 56.0° with the plane of the phosphazene ring. The length of the normal from the cyclopentadienyl ring to the cobalt atom is 1.71 Å.

The structures of **6** and **7** are similar and are shown in Figures 5 and 6. The molecules of **6** and **7** contain phosphazene-bridged dicobalt and dirhodium units. In both molecules, each metal atom bears a cyclopentadienyl ring and a terminal carbonyl ligand. The cyclopentadienyl rings are disposed in a trans orientation about the metal–metal axis, as expected for a dimetallic dimer with a large bridging function—such as a phosphazene ring. In **6** and **7**, the planes defined by the two cyclopentadienyl rings are not parallel (dihedral angle = 35.9° for **6** and 35.5° (average) for **7**), giving rise to a distortion of the idealized C_{2v} symmetry. The Co(1)–Co(2) bond length of 2.552 Å in **6** compares well with the related dimer $Co_2Cp_2(PPh_2)_2$ in which the Co–Co distance is 2.56 Å.[31] The average distance from the bound cyclopentadienyl ring to each cobalt (normal vector) in **6** is 1.70 Å. The Rh(1)–Rh(2) bond distance in **7** is 2.747 Å (average). This is in agreement with values reported for Rh–Rh single bonds in other compounds (2.62–2.84 Å).[32-39] The average distance from

(28) Dahl, L. F.; Martell, C.; Wampler, D. L. *J. Am. Chem. Soc.* **1961**, *83*, 1761.
(29) Teo, B. K.; Hall, M. B.; Fenske, R. F.; Dahl, L. F. *Inorg. Chem.* **1975**, *14*, 3103 and references cited therein.
(30) Keller, E.; Vahrenkamp, H. *Angew. Chem., Int. Ed. Engl.* **1977**, *16*, 542.
(31) Coleman, J. M.; Dahl, L. F. *J. Am. Chem. Soc.* **1967**, *89*, 542.
(32) Corey, E. R.; Dahl, L. F.; Beck, W. *J. Am. Chem. Soc.* **1963**, *85*, 1202.
(33) Wei, C. H. *Inorg. Chem.* **1969**, *8*, 2384.
(34) Mills, O. S.; Nice, J. P. *J. Organomet. Chem.* **1967**, *10*, 337.
(35) Mills, O. S.; Paulus, E. F. *J. Organomet. Chem.* **1967**, *10*, 331.
(36) Paulus, E. F. *Acta Crystallogr., Sect. B.* **1969**, *B25*, 2206.
(37) Cowie, M.; Mague, J. T.; Sanger, A. R. *J. Am. Chem. Soc.* **1978**, *100*, 3628.
(38) Cowie, M. *Inorg. Chem.* **1979**, *18*, 286.
(39) Eisenberg, R.; Kubiak, C. P. *J. Am. Chem.* Soc. **1980**, *102*, 3637.

Table XIV. Bond Angles (deg) for 7

	A	B
Rh(1)-Rh(2)-P(1)	52.75 (8)	51.09 (8)
Rh(2)-Rh(1)-P(1)	50.73 (8)	53.71 (8)
Rh(1)-P(1)-Rh(2)	76.5 (1)	75.2 (1)
Rh(1)-P(1)-N(1)	119.5 (4)	119.3 (3)
Rh(1)-P(1)-N(3)	113.3 (3)	113.5 (4)
Rh(2)-P(1)-N(1)	115.0 (4)	114.5 (3)
Rh(2)-P(1)-N(3)	117.1 (4)	119.4 (4)
Rh(1)-Rh(2)-C(2)	88.4 (5)	89.0 (5)
Rh(2)-Rh(1)-C(1)	89.3 (4)	91.7 (5)
P(1)-Rh(1)-C(1)	93.6 (4)	90.1 (4)
P(1)-Rh(2)-C(2)	89.6 (5)	90.5 (5)
N(1)-P(1)-N(3)	111.6 (5)	111.0 (5)
N(1)-P(2)-N(2)	119.7 (4)	120.7 (5)
N(2)-P(3)-N(3)	119.7 (5)	119.6 (5)
P(1)-N(1)-P(2)	124.4 (6)	123.4 (5)
P(2)-N(2)-P(3)	115.6 (6)	116.4 (6)
P(1)-N(3)-P(3)	121.7 (5)	122.6 (6)
Cl(1)-P(2)-Cl(2)	99.7 (2)	100.0 (2)
Cl(3)-P(3)-Cl(4)	100.9 (2)	99.5 (2)
Cl(1)-P(2)-N(1)	107.4 (4)	108.8 (4)
Cl(1)-P(2)-N(2)	109.5 (5)	108.5 (5)
Cl(2)-P(2)-N(1)	112.3 (4)	110.2 (4)
Cl(2)-P(2)-N(2)	106.4 (5)	106.6 (5)
Cl(3)-P(3)-N(2)	105.8 (4)	108.6 (4)
Cl(3)-P(3)-N(3)	109.7 (4)	108.3 (4)
Cl(4)-P(3)-N(2)	109.7 (5)	106.2 (5)
Cl(4)-P(3)-N(3)	109.3 (4)	112.7 (4)
Rh(1)-C(1)-O(1)	174 (1)	176 (1)
Rh(2)-C(2)-O(2)	176 (2)	176 (1)
C(12)-C(11)-C(15)	110 (1)	109 (1)
C(11)-C(12)-C(13)	105 (1)	108 (1)
C(12)-C(13)-C(14)	108 (1)	106 (1)
C(13)-C(14)-C(15)	108 (1)	109 (1)
C(11)-C(15)-C(14)	109 (1)	107 (1)
C(22)-C(21)-C(25)	111 (1)	107 (2)
C(21)-C(22)-C(23)	107 (1)	109 (2)
C(22)-C(23)-C(24)	106 (2)	108 (1)
C(23)-C(24)-C(25)	111 (1)	107 (2)
C(21)-C(25)-C(24)	105 (1)	108 (1)

the cyclopentadienyl ring to each rhodium atom (normal vector) in **7** is 1.91 Å.

The phosphazene rings in **5–7** show substantial deviation from planarity (χ^2 = 1270, 4429, and 1269 (average), respectively). All the compounds contain bulky cyclopentadienyl rings which undoubtedly generate distortions via crystal packing forces. The dihedral angles between the idealized phosphazene ring and the metal–metal–P(1) plane are 82.7° (**5**), 84.3° (**6**), and 80.6° (average) (**7**). The dihedral angle in the dirhodium species shows the greatest deviation from orthogonality. As expected for these dimetallophosphazenes, the plane defined by the three-membered spiro rings passes through the distal nitrogen atom N(2) (with a deviation of less than 1°).

The skeletal phosphorus atoms in cyclic phosphazenes usually assume a distorted tetrahedral geometry, with a ring angle near 120° and an exocyclic angle near 100°.[40] The metal–P(1)–metal bonding angles in **5**, **6**, and **7** lie in the range of 73–76°. (The increase in this angle in the series **5**, **6**, and **7** parallels the increase in the metal–metal bonding distances.) Also, the N(1)–P(1)–N(3) angles are constricted to the 111–112° range. What is peculiar about this geometry is the contraction of both the metal–P–metal and N–P–N angles at the organometallic bridgehead. Thus, although it might be argued that bulky, mutually repelling side groups might widen the R–P–R angle and narrow the N–P–N angle by a "scissor" effect,[41] such an explanation is clearly impossible when the R–P–R angle is narrowed in response to the constraints of the exocyclic three-membered ring. In structures **5–7** and in related metallophosphazenes[16-18] it must be inferred that powerful electronic interactions between the metallo units and the phosphazene bring about the skeletal distortion. The other endocyclic angles centered at P(2) and P(3) are similar to those found in $(NPCl_2)_3$ (~120°).[40]

Within the phosphazene ring in compounds **5–7**, the two P–N bonds proximal to the metal atoms are the longest. The adjacent pair of P–N bonds are the shortest, and those furthest from the metal atoms are of intermediate length. Thus, the bond length variations in **5**, **6**, and **7** are are follows: P(1)–N(1) or P(1)–N(3) = 1.62–1.64 Å; P(2)–N(1) or P(3)–N(3) = 1.53–1.56 Å; P(2)–N(2) or P(3)–N(2) = 1.57–1.59 Å (see Tables VII, X, and XIII for specific values). The lengths of the P–N bonds furthest from P(1) are very similar to those found in $(NPCl_2)_3$.[40] This pattern of bond length variation has been detected in other asymmetrically substituted cyclophosphazenes.[16-18,41] The effect has been attributed to variations in the π bonding within the phosphazene ring, caused by the less electronegative substituents at P(1).

Other common structural features of interest in compounds **5–7** include the following: (1) the endocyclic bond angles centered at N(1) and N(3) lie in the range 122–124°, whereas the distal angle centered at N(2) is contracted (116–117°); (2) the exocyclic Cl–P(2 or 3)–Cl angles (99–101°) are similar to those found in $(NPCl_2)_3$;[40] (3) the acute endocyclic P(1)–M(1)–M(2) and P(1)–M(2)–M(1) angles lie in the range 51–54°; (4) the Fe–P(1) bond length (2.20 Å) and the Co–P(1) bond lengths (average 2.14 Å) are in good agreement with values for related compounds[30,31] (the Rh–P(1) bond lengths average 2.23 Å).

Conclusions. Although metal scrambling reactions are well-known in conventional transition metal systems,[42-49] the transformations that lead to compounds **4–7** are new and unusual. The pentavalent phosphorus atom in a phosphazene ring participates mainly in the formation of covalent bonds. In this regard it differs from the well-documented roles of phosphorus in phosphine complexes or phosphido-bridged organometallic compounds where coordinative bonding is more typical. We infer that cobalt has a stronger tendency to bond to phosphorus in these structures but that iron bonds to the most basic site, which is a skeletal nitrogen atom.

The exact reaction mechanisms operative in these transformations are not known. One possibility is that the cobalt completely displaces iron from phosphorus, leaving $Fe(CO)_4THF$ to seek the most basic site on the phosphazene ring. Alternatively, the first step may involve the addition of a coordinatively unsaturated metal carbonyl fragment to a phosphorus-bound metal fragment. This interaction may be promoted by a thermally induced metal–metal bond cleavage process in **2** (or **5**). Rearrangement and expulsion of another fragment could then occur to yield the reaction products. The possibility exists

(40) Allcock, H. R. "Phosphorus-Nitrogen Compounds"; Academic Press: New York, 1972.
(41) Allcock, H. R.; Connolly, M. S.; Whittle, R. R. *Organometallics* **1983**, *2*, 1514.
(42) Vahrenkamp, H.; Wucherer, E. J. *Angew. Chem., Int. Ed. Engl.* **1981**, *20*, 680.
(43) Beurich, H.; Vahrenkamp, H. *Angew. Chem., Int. Ed. Engl.* **1978**, *11*, 863.
(44) Madach, T.; Vahrenkamp, H. *Chem. Ber.* **1980**, *113*, 2675.
(45) Beurich, H.; Vahrenkamp, H. *Angew. Chem., Int. Ed. Engl.* **1981**, *1*, 98.
(46) Wrighton, M. S.; Ginley, D. S. *J. Am. Chem. Soc.* **1975**, *97*, 4246.
(47) Abrahamson, H. B.; Gray, H. B.; Wrighton, M. S. *Inorg. Chem.* **1977**, *16*, 1554.
(48) Abrahamson, H. B.; Wrighton, M. S. *Inorg. Chem.* **1978**, *17*, 1003.
(49) Johnson, B. F. G.; Lewis, J.; Matheson, T. W. *J. Chem. Soc., Chem. Commun.* **1974**, 441.

Table XV. Fractional Atomic Positional Parameters for 7

	A			B		
	x	*y*	*z*	*x*	*y*	*z*
Rh(1)	0.4689 (1)	0.09553 (8)	0.40760 (4)	0.5259 (1)	0.58547 (9)	0.09112 (4)
Rh(2)	0.5211 (1)	0.02419 (9)	0.30996 (4)	0.4607 (1)	0.54528 (9)	0.18859 (4)
P(1)	0.4836 (3)	−0.1073 (3)	0.3728 (1)	0.5052 (3)	0.3931 (3)	0.1264 (1)
P(2)	0.6418 (3)	−0.3956 (3)	0.3853 (1)	0.3423 (4)	0.1887 (3)	0.1157 (1)
P(3)	0.2855 (3)	−0.2797 (3)	0.3999 (1)	0.7001 (4)	0.1168 (3)	0.1016 (1)
Cl(1)	0.7905 (4)	−0.4931 (3)	0.4383 (1)	0.2114 (4)	0.1439 (4)	0.1753 (1)
Cl(2)	0.7767 (5)	−0.5159 (4)	0.3275 (1)	0.1902 (5)	0.1637 (4)	0.0643 (1)
Cl(3)	0.0831 (4)	−0.3210 (3)	0.3735 (2)	0.8995 (4)	−0.0278 (3)	0.1305 (1)
Cl(4)	0.2050 (5)	−0.2572 (4)	0.4716 (1)	0.7851 (5)	0.0917 (4)	0.0302 (1)
N(1)	0.652 (1)	−0.2463 (8)	0.3814 (4)	0.333 (1)	0.3440 (9)	0.1175 (4)
N(2)	0.453 (1)	−0.4183 (9)	0.3922 (5)	0.528 (1)	0.0685 (9)	0.1081 (5)
N(3)	0.296 (1)	−0.1405 (8)	0.3788 (4)	0.691 (1)	0.2606 (9)	0.1212 (4)
O(1)	0.860 (1)	0.020 (1)	0.4162 (4)	0.141 (1)	0.680 (1)	0.0724 (5)
O(2)	0.130 (1)	0.140 (1)	0.3016 (5)	0.848 (1)	0.453 (1)	0.2029 (5)
C(1)	0.716 (2)	0.044 (1)	0.4110 (5)	0.283 (2)	0.644 (1)	0.0809 (6)
C(2)	0.278 (2)	0.093 (1)	0.3060 (6)	0.704 (2)	0.490 (2)	0.1957 (6)
C(11)	0.241 (2)	0.137 (1)	0.4645 (6)	0.817 (2)	0.548 (2)	0.0842 (6)
C(12)	0.177 (2)	0.197 (1)	0.4209 (7)	0.770 (2)	0.511 (1)	0.0398 (6)
C(13)	0.254 (2)	0.310 (1)	0.4112 (6)	0.650 (2)	0.631 (2)	0.0198 (5)
C(14)	0.364 (2)	0.305 (1)	0.4476 (6)	0.631 (2)	0.744 (1)	0.0541 (7)
C(15)	0.359 (2)	0.196 (1)	0.4795 (5)	0.733 (2)	0.694 (2)	0.0916 (6)
C(21)	0.749 (2)	−0.116 (1)	0.2627 (6)	0.165 (2)	0.630 (2)	0.2011 (6)
C(22)	0.816 (2)	−0.036 (2)	0.2942 (5)	0.224 (2)	0.526 (1)	0.2324 (6)
C(23)	0.744 (2)	0.103 (2)	0.2804 (6)	0.332 (2)	0.562 (2)	0.2644 (5)
C(24)	0.634 (2)	0.106 (2)	0.2429 (5)	0.336 (2)	0.696 (2)	0.2516 (7)
C(25)	0.632 (2)	−0.032 (2)	0.2335 (5)	0.231 (2)	0.742 (2)	0.2144 (8)

that the phosphazene passes through a transition state stabilized by a phosphorus–metal double bond. Such a process would have interesting implications for the use of these compounds as catalyst precursors. As yet, the catalytic properties of these compounds are unknown.

It is possible that compounds **2** and **5** (or even **6** and **7**) could react with a variety of other neutral metal carbonyl compounds to yield stable mixed-metal products or metal substitution products. Two important factors govern the outcome of reactions of this type: (1) the rates of decomposition of the starting materials (by loss of CO or by metal–metal bond cleavage) should be comparable and (2) the formation of metal–metal bonds should be a favored process to provide a driving force for the construction of metal–metal bonded frameworks. The possibility exists that phosphazene cluster compounds that contain more than three metal atoms could be prepared. In addition, the use of compound **5** in reactions with neutral metal carbonyls provides a route for the formation of metallophosphazenes that possess three or four different metal atoms in a cluster framework.

The long-range goal of this work is to carry out similar reactions with the use of linear, high molecular weight, poly(dichloro- or difluorophosphazene) as the initial substrate. Macromolecular reactions are always more complex than those of their small-molecule counterparts. Nevertheless, some potentially simplifying features have emerged from the small molecule studies.

First, the metal-exchange reactions reported here for the trimer provide a route to the synthesis of a diverse range of different metallo derivatives of the high polymer—starting from a seemingly accessible iron carbonyl derivative analogous to **2**.

Second, at the cyclic trimer level, the introduction of a metallo unit deactivates the two flanking PCl_2 residues to further substitution in **2**. If this phenomenon persists in the high polymer, it suggests a mechanism for the controlled, partial introduction of metallo species. This provides an opportunity for defining the conformation of the polymer in the solid state and assisting controlled intramolecular decarbonylation reactions that would allow the construction of a one-dimensional metallo polymer, stabilized by the polyphosphazene template. We are currently exploring these possibilities.

Experimental Section

Materials. All experimental manipulations were performed under an atmosphere of dry nitrogen (Matheson). $N_3P_3Cl_4Fe_2(CO)_8$ (**2**) was prepared from $(NPCl_2)_3$ (Firestone Tire and Rubber Co.) and $Na_2Fe_2(CO)_8$[50] using methods described previously.[18] $RhCp(CO)_2$ was prepared from $[RhCl(CO)_2]_2$ (Strem Chemicals, Inc.) and NaC_5H_5 in hexane according to a variation of a literature method.[51] $Co_2(CO)_8$ and $CoCp(CO)_2$ were commercial products obtained from Strem Chemicals, Inc., and were used as received. Hexane and heptane (Fisher) were distilled from calcium hydride before use. Two grades of silica gel were used: coarse (23–200 mesh, Davison Chemical) and fine (230–400 mesh ASTM, EM Reagents).

Equipment. ^{31}P NMR spectra were obtained by means of a Bruker WP-200 FT NMR spectrometer operating at 80 MHz. ^1H NMR data were obtained with the use of the same spectrometer operating at 200 MHz. Infrared spectra were recorded with the use of a Perkin-Elmer 283B infrared spectrophotomer or a Perkin-Elmer 580 grating spectrophotometer. Mass spectrometric analyses were performed with the use of a Finnegan 3200 or an AEI MS 902 spectrometer. Microanalyses were obtained by Galbraith Laboratories, Knoxville, Tenn.

Mössbauer spectra were recorded with a constant acceleration spectrometer. The samples[52] were mounted on the cold finger of a liquid-nitrogen-cooled cryostat at a temperature of 77 K.[53] Doppler shifts were calibrated with an iron foil, and all velocities are given relative to the centroid of metallic iron at 300 K. All the spectra were fitted with Lorentzian-shaped quadrupole pairs, with the isomer shifts, the quadrupole splitting, the half-width at half maximum of the Lorentzians, and the area of the quadrupole pairs as parameters. A nonlinear least-squares Fortran computer program[54] was used to facilitate the fitting. The solid

(50) Collman, J. P.; Finke, R. G.; Matlock, P. L.; Wahren, R.; Brauman, J. I. *J. Am. Chem. Soc.* **1976**, *98*, 4685.
(51) Bittler, K.; Fischer, E. O. *Z. Naturforsch. B: Anorg. Chem., Org. Chem., Biochem., Biophys. Biol.* **1961**, *16B*, 225.
(52) Samples were prepared by forming a homogeneous mixture of the solid product with an inert substance (boron nitride) using a mortar and pestle).
(53) Lang, G. *Q. Rev. Biophys.* **1970**, *3*, 1.

lines in Figure 2 are the output of the program.

X-ray crystallographic analyses are described in a later section.

Synthesis of $N_3P_3Cl_4Co_2Fe(CO)_9$ (4). Compound **2** (0.85 g, 1.4 mmol) and $Co_2(CO)_8$ (1.0 g, 2.9 mmol) were combined in a 200-mL Schlenk flask. Freshly distilled hexane (100 mL) was added, and the solution was heated at reflux for 5 h. After the solution had cooled to ambient temperature, the contents were applied to a silica gel (coarse) column packed with hexane. Elution with hexane yielded first a brown band containing unreacted $Co_2(CO)_8$, followed by a purple-brown band containing **4** (0.1 g, ~10%). Unreacted **2** (0.7 g, ~82%) was recovered by subsequent elution with methylene chloride. Removal of the solvent from the second fraction yielded a brown crystalline solid, **4**. Mass spectrum for **4**: m/e(calcd) 701, m/e(found) 701. Anal. Calcd for $Co_2FeCl_4P_3O_9N_3C_9$: Fe, 7.95; Co, 16.78; C, 15.39; P, 13.23. Found: Fe, 7.72; Co, 16.61; C, 15.91; P, 12.92.

Synthesis of $N_3P_3Cl_4FeCoCp(CO)_5$ (5) and $N_3P_3Cl_4Co_2Cp_2(CO)_2$ (6). Compound **2** (1.3 g, 2.1 mmol) was dissolved in dry hexane (100 mL) in a 200-mL Schlenk flask. $CoCp(CO)_2$ (1.5 mL, ~8 mmol) was then added via syringe. The mixture was heated at reflux for 14 h and was then allowed to cool to ambient temperature. The reaction mixture was then applied to a silica gel (coarse) column containing hexane. Elution with hexane resulted in the separation of unreacted $CoCp(CO)_2$. (Some decomposition of the $CoCp(CO)_2$ occurred during the chromatographic separation, causing the column to turn a dark blue.) Subsequent elution with methylene chloride eluted a mixture of **2**, **5**, and **6** as a dark fraction. The solvent was removed from this mixture by rotary evaporation. The solid residue was then redissolved in methylene chloride (15%)/hexane (85%) and was applied to a silica gel (fine) column that had been packed with the same solvent mixture. Unreacted **2** (0.4 g, ~31%) separated as an orange band following elution with methylene chloride (15%)/hexane (85%). The remaining dark band was separated into two bands by subsequent elution with a methylene chloride (30%)/hexane (70%) solvent mixture. Compound **5** was collected as the first maroon fraction, which yielded a red-brown crystalline solid after removal of the solvent by rotary evaporation (0.55 g, ~44%). The remaining brown fraction was then quickly eluted with pure methylene chloride, yielding a brown crystalline solid after removal of the solvent. This material consisted of **6** (0.05 g, ~4%). Mass spectrum for **5**: m/e(calcd) 594.6877, m/e(found) 594.6844. Mass spectrum for **6**: m/e(calcd) 579, m/e(found) 579. Anal. Calcd for $CoFeCl_4P_3O_5N_3C_{10}H_5$: Fe, 9.36; Co, 9.88; N, 7.04; C, 20.13; H, 0.84. Found: Fe, 9.65; Co, 9.31; N, 6.89; C, 20.88; H, 0.94. ^{1}H NMR: **5**, δ 5.26 (s); **6**, δ 5.11 (s) (in $CDCl_3$ with Me_4Si reference).

Reaction of $N_3P_3Cl_4FeCoCp(CO)_5$ (5) with $CoCp(CO)_2$. Compound **5** (0.4 g, 0.7 mmol) was placed in a 200-mL Schlenk flask. Hexane (100 mL) was added, followed by $CoCp(CO)_2$ (1 mL, ~5.6 mmol). The reactants were heated at reflux for 18 h and then were allowed to cool to ambient temperature. Chromatographic separation of the components by the procedure described in the preceding section resulted in the separation of **5** (0.3 g, ~75% recovered) from **6** (0.035 g, ~9%). Higher yields (~45%) of **6** could be obtained if the reaction was carried out by using heptane as the reaction solvent.

Reaction of $N_3P_3Cl_4Fe_2(CO)_8$ (2) with $RhCp(CO)_2$. A solution of $RhCp(CO)_2$ was prepared by allowing $[RhCl(CO)_2]_2$ (0.5 g, 1.3 mmol) to react with a tenfold excess of NaC_5H_5 (1.13 g, 13.0 mmol) in dry, deoxygenated hexane (~20 mL). The reaction mixture was stirred at ambient temperature for several hours and then heated at reflux for ~1 h. The reaction mixture was then allowed to cool to ambient temperature, and the orange $RhCp(CO)_2$ solution was transferred to a coarse-fritted addition funnel and was added dropwise to a solution of compound **2** (0.27 g, 0.4 mmol) in dry, deoxygenated hexane (~25 mL). The reaction mixture was then heated at reflux for ~1 h.

The solution was allowed to cool to ambient temperature and was then applied to a silica gel (coarse) column packed with hexane solvent. Elution with hexane yielded first an orange band containing $RhCp(CO)_2$. Unreacted **2** was recovered by elution with a methylene chloride (25%)/hexane (75%) solvent mixture. A third, red-orange band containing **7** was eluted with methylene chloride (50%)/hexane (50%). Removal of the solvent from the third band yielded a red-orange crystalline solid, $N_3P_3Cl_4Rh_2Cp_2(CO)_2$ (**7**). Mass spectrum for **7**: m/e(calcd) 666.6836, m/e(found) 666.6856. Anal. Calcd for $Rh_2Cl_4P_3O_2N_3C_{12}H_{10}$: Rh, 30.77; N, 6.28; P, 13.89; C, 21.55; H, 1.51. Found: Rh, 31.08; N, 6.13; P, 13.83; C, 21.67; H, 1.49. ^{1}H NMR: δ 5.6 (s) (in $CDCl_3$ with Me_4Si reference).

Reaction of $N_3P_3Cl_4FeCoCp(CO)_5$ (5) with $RhCp(CO)_2$. A solution of $RhCp(CO)_2$, prepared in a manner identical with that described above, was added dropwise through a coarse-fritted funnel into a solution of compound **5** (0.30 g, 0.50 mmol) in dry, deoxygenated hexane (~25 mL). The reaction mixture was then heated at reflux for 12 h.

The reaction mixture was then allowed to cool to ambient temperature, and the solution was applied to a silica gel (coarse) column packed in hexane. Elution with hexane yielded an orange band containing $RhCp(CO)_2$. The remainder of the material on the column was removed as one dark reddish brown band with methylene chloride. This band contained a mixture of compounds **5** and **7**. The methylene chloride was removed from this fraction by rotary evaporation. The solids were then redissolved in methylene chloride (15%)/hexane (85%), and the solution was applied to a silica gel (fine) column packed with the same solvent mixture. Unreacted **5** was eluted with methylene chloride (15%)/hexane (85%) which separated as a maroon band. The remaining red-orange band containing **7** was eluted with methylene chloride (30%)/hexane (70%). Removal of the solvent from this band gave **7** (by IR, mass spectrum, ^{31}P NMR) in ~40% yield.

X-ray Structure Determination. (a) Crystal Preparation. Crystals of each compound **4**–**7** were grown from the solvents indicated in Table III. The general procedure used for growing suitable crystals was the following: the compound was dissolved in a minimum amount of solvent in a small flask and was placed in a Dewar insulator which contained a small quantity of water. This whole assembly was covered and placed in a freezer to ensure slow cooling of the solution. After crystal formation had occurred, a suitable crystal (see Table III for approximate crystal dimensions) was mounted with epoxy cement on a glass fiber (approximately one-fourth the crystal diameter).

(b) Data Collection. A given crystal was optically centered on an Enraf-Nonius four-circle CAD4 automated diffractometer controlled by a PDP8/a computer coupled to a PDP11/34a computer. A full-rotation orientation photograph was taken with a Polaroid cassette accessory, and 25 rather intense reflections were chosen and centered with the use of manufacture-supplied software.[55] The INDEX program was used to obtain an orientation matrix and unit cell parameters. Successive centerings and least-squares refinements of 2θ values found for the 25 precisely centered reflections gave the lattice constants listed in Table III for each of the four crystals. Program TRACER was used to determine the appropriateness of the unit cell chosen initially. A small test data set (axial and zero layer reflections) was collected to determine the systematic absences, if any. The space group in each case was determined to be $P\bar{1}$ (Table III) and was confirmed by the successful refinement of each structure. The number of formula units per unit cell, Z (Table III), was determined on the basis of the measured density of each compound.

A graphite single-crystal incident beam monochromator was used for data collection at room temperature (21 °C) with Mo Kα radiation (λ = 7.1073 Å) (takeoff angle 2.8°). A θ–2θ scan method was used with 2θ ranging from $(A + 0.347 \tan \theta)°$ below the calculated position of the Kα_1 reflection to $(A + 0.347 \tan \theta)°$ above the calculated position of the Kα_2 reflection. The A values are given in Table III. The scan rate was varied automatically ranging from 5°/min for the most intense reflections to 1°/min for the weak ones. Background counts were measured with the detector stationary and positioned at the beginning and end of the scan, each for 25% of the total scan time. During the data collection, three standard reflections were measured after periodic intervals of X-ray exposure time and were recentered automatically after every several hundred reflections to monitor

(54) See, for example: Chrisman, B. L.; Tumolillo, T. A. *Comput. Phys. Commun.* **1971**, *2*, 322.

(55) All programs used in the data collection, reduction, and refinement are part of the: "Enraf-Nonius Structure Determination Package"; Enraf-Nonius; Delft, The Netherlands, 1975, revised 1977.

crystal orientation and stability. In all cases, the standard reflections were used to rescale the data automatically to correct the drift during data collection. Drift corrections were random and long term and are indicated in Table III. The total number of unique reflections measured, and their numbers with respect to the standard deviation in intensity, $\sigma(I)$, are given in Table III for each compound, with the criterion for observation being $I > 2\sigma(I)$. The integrated intensity, I, was calculated according to the expression[56] $I = [SC - 2(B_1 + B_2)]T_R$, where SC is the scan count, B_1 and B_2 are the background counts at each end of the scan, and T_R is the 2θ scan rate in degrees per minute. The unique, normalized, integrated intensity set was processed to give F and E values. Lorentz and polarization corrections[55] were applied in the determination of the structure factor amplitudes. Linear absorption coefficients (μ, cm^{-1}) for Mo Kα radiation are given in Table III. The values were sufficiently small that no absorption corrections were applied.

Structure Solution and Refinement. The positions of the metal atoms in each case were established from a sharpened, origin-removed Patterson map and were confirmed by a direct method solution. The remaining non-hydrogen atoms were located with one or two additional Fourier syntheses. All non-hydrogen atoms were refined anisotropically. The number of parameters, including overall scale factor, positional parameters, and anisotropic thermal parameters,[26] varied in each case and are listed in Table III. Hydrogen atoms for compounds **5–7** were located at their calculated positions. All hydrogen atoms were assigned fixed isotropic temperature parameters[57] of $B = 5.0$ Å^2. None of the parameters for the hydrogen atoms were varied. Neutral-atom scattering factors were those by Cromer and Mann[58] and by Stewart et al.[59] for non-hydrogen atoms and hydrogen atoms, respectively. Real and imaginary anomalous dispersion corrections to the atomic scattering factors were included.[60] In the last cycle of least-squares refinement the maximum parameter shift was less than 0.33 of a standard deviation. The final R values[61] are listed in Table III. Final difference Fourier maps showed the residual electron density (e Å^{-3}) for each structure, as indicated in Table III.

Acknowledgment. We thank the U.S. Army Research Office for the support of this work. We also thank L. G. Lang for the Mössbauer data: The Mössbauer work was supported by the National Institutes of Health through Grant no. HL-16860. The NMR data were obtained by R. A. Nissan and J. L. Desorcie.

Registry No. **2**, 83437-98-3; **4**, 94042-46-3; **5**, 94042-47-4; **6**, 94042-48-5; **7**, 94042-49-6; $Co_2(CO)_8$, 10210-68-1; $CoCp(CO)_2$, 12078-25-0; $RhCp(CO)_2$, 12192-97-1; $[RhCl(CO)_2]_2$, 14523-22-9.

Supplementary Material Available: Listing of thermal parameters, root-mean-square displacements, and observed and calculated structure factors for compounds **4**, **5**, **6**, and **7** (54 pages). Ordering information is given on any current masthead page.

(56) Corfield, P. W. R.; Doedens, R. J.; Ibers, J. A. *Inorg. Chem.* **1967**, *6*, 197.
(57) Isotropic thermal parameters are of the form $\exp[-B(\sin^2\theta)/\lambda^2]$.
(58) Cromer, D. T.; Mann, J. B. *Acta Crystallogr., Sect. A* **1968**, *A24*, 321.
(59) Stewart, R. F.; Davidson, E. R.; Simpson, W. T. *J. Chem. Phys.* **1965**, *42*, 3175.
(60) "International Tables for X-Ray Crystallography", 3rd. ed.; Kynoch Press: Birmingham, U.K., 1968; Vol. III, Table 3.3.2C, pp 2115–2116.
(61) $R_1 = \sum||F_o| - |F_c||/\sum|F_o|$; $R_2 = [\sum w(|F_o| - |F_c|)^2/\sum w(F_o)^2]^{1/2}$; $w = 1/\sigma(F_o)^2$.

Proton Affinities of Pyridine, Phosphabenzene, and Arsabenzene†

Ronald V. Hodges,[1a,c] J. L. Beauchamp,*[1a] Arthur J. Ashe, III,*[1b] and W.-T. Chan[1b]

Arthur Amos Noyes Laboratory of Chemical Physics, California Institute of Technology, Pasadena, California 91125, and the Department of Chemistry, The University of Michigan, Ann Arbor, Michigan 48109

Received July 10, 1984

The proton affinities of phosphabenzene and arsabenzene are determined by ion cyclotron resonance techniques to be 195.8 and 189.3 kcal/mol, respectively, relative to $PA(NH_3)$ = 203.6 kcal/mol. These values are compared to those of pyridine, 219.4 kcal/mol, and other group 5 compounds. Deuterium labeling experiments demonstrate that phosphabenzene is protonated on the phosphorus atom, and arsabenzene is protonated on carbon.

Introduction

The group 5 heterobenzenes, pyridine **1**, phosphabenzene **2**,[2,3] arsabenzene **3**,[2-4] stibabenzene **4**,[3-6] and bismabenzene **5**,[3,4,6,7] form a unique series in which elements from

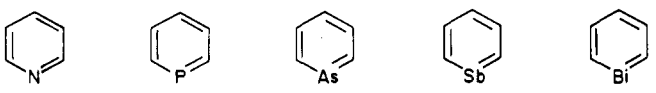

1 2 3 4 5

an entire column of the periodic table have been incorporated into aromatic rings. Spectroscopic studies have indicated that there are great similarities in aromatic character of the entire series.[3,4] However, chemical studies have shown a marked divergence of the heavier heterobenzenes from pyridine.[3,4]

In particular, the chemistry of pyridine is dominated by the basicity of the nitrogen atom. However, the heteroatoms of phosphabenzene and arsabenzene do not show basic properties in solution (**2** ↛ **6**)[8] nor are they quater-

† Contribution No. 5680.

(1) (a) California Institute of Technology. (b) The University of Michigan. (c) N.S.F. Graduate Fellow (1973–1976).
(2) Ashe, A. J., III *J. Am. Chem. Soc.* **1971**, *93*, 3293.
(3) Ashe, A. J., III *Acc. Chem. Res.* **1978**, *11*, 153.
(4) Ashe, A. J., III *Top. Curr. Chem.* **1982**, *105*, 125.
(5) Ashe, A. J., III *J. Am. Chem. Soc.* **1971**, *93*, 6690.
(6) Ashe, A. J., III; Diephouse, T. R.; El-Sheikh, M. Y. *J. Am. Chem. Soc.* **1982**, *104*, 5693.
(7) Ashe, A. J., III; Gordon, M. D. *J. Am. Chem. Soc.* **1972**, *94*, 7596.
(8) Smith, T. W. Ph.D. Thesis, The University of Michigan, 1977.

0276-7333/85/2304-0457$01.50/0